Dynamics of the Metallo-β-Lactamase from *Bacteroides fragilis* in the Presence and Absence of a Tight-Binding Inhibitor[†]

James J. A. Huntley, Sergio D. B. Scrofani,[‡] Michael J. Osborne,[§] Peter E. Wright, and H. Jane Dyson*

Department of Molecular Biology and Skaggs Institute for Chemical Biology, The Scripps Research Institute, 10550 North Torrey Pines Road, La Jolla, California 92037

Received May 26, 2000; Revised Manuscript Received August 28, 2000

ABSTRACT: A significant determinant for the broad substrate specificity of the metallo-β-lactamases from *Bacteroides fragilis* and other similar organisms is the presence of a plastic substrate binding site that is nevertheless capable of tight substrate binding in the Michaelis complex. To achieve these two competing ends, the molecule apparently employs a flexible flap that closes over the active site in the presence of substrate. These characteristics imply that dynamic changes are an important component of the mechanism of action of these enzymes. The backbone and tryptophan side chain dynamics of the metallo-β-lactamase from *B. fragilis* have been examined using ^{15}N NMR relaxation measurements. Two states of the protein were examined, in the presence and absence of a tight-binding inhibitor. Relaxation measurements were analyzed by the model-free method. Overall, the metallo-β-lactamase molecule is rigid and shows little flexibility except in loops. The flexibility of the loop that covers the active site is not unusually great as compared to the other loops of the protein. Local motion on a picosecond time scale was found to be very similar throughout the protein in the presence and absence of the inhibitor, but a significant difference was observed in the motions on a nanosecond time scale (τ_e). Large-amplitude motions with a time constant of about 1.3 ns were observed for the flexible flap region (residues 45−55) in the absence of the inhibitor. These motions were completely damped out in the presence of the inhibitor. In addition, the motion of a tryptophan side chain at the tip of the β-hairpin of the flap shows a very significant difference in motion on the ps time scale. These results indicate that the motions of the polypeptide chain in the flap region can be invoked to explain both the wide substrate specificity (the free form has considerable amplitude of motion in this region) and the catalytic efficiency of the metallo-β-lactamase (the motions are damped out when the inhibitor and by implication a substrate binds in the active site).

Since their discovery in the late 1940s, antibiotics have been widely used to eradicate harmful bacterial infections in humans without causing deleterious side effects. Although varied in their targets, antibiotics generally slow the proliferation of bacteria by interfering with the production of components needed to form new bacterial cells. For example, tetracycline affects bacterial protein synthesis through interactions with ribosomes, while penicillin and vancomycin retard bacterial growth by inhibiting transpeptidase activity necessary for bacterial cell wall synthesis (*1*). However, evidence is mounting concerning the recent emergence of pathogenic bacteria that have displayed marked resistance to commonly used antibiotics (*2*−*4*). The appearance of these antibiotic-resistant bacteria represents a considerable public health concern and has heightened awareness regarding the proliferation and treatment of disease associated with such organisms (*5*).

The most common cause of antibiotic resistance is through the bacterial production of enzymes that intercept and degrade popular β-lactam-based antibiotics, such as penicillin. Though problematic, there exist several strategies to address the resistance afforded by the production of β-lactamases. Structural alterations to existing drugs can be made to make them less susceptible to degradation. Alternatively, agents can be designed to incapacitate the β-lactamase in concert with existing antibiotics. Although there has been some success in treating bacterial infections associated with a number of specific β-lactamases (*6*), recently developed antibiotics have displayed only limited therapeutic effect (*7*). Therefore, defining and establishing novel combative strategies is critical for the continued use of β-lactams as antibacterial agents.

Four major classes of β-lactamases have been identified and grouped based upon amino acid sequence similarities (*6*, *8*, *9*). Classes 1, 2, and 4 are serine hydrolases and have been shown to be inhibited by compounds such as sulbactam and clavulanic acid (*6*). Group 3 enzymes include all of the metal-requiring (metallo) β-lactamases that hydrolyze all β-lactam antibiotics but show little susceptibility to presently used β-lactamase inhibitors.

Approximately 10 organisms have currently been shown to produce metallo-β-lactamases, including *Klebsiella* (*4*),

[†] This work was supported by Grant GM56879 from the National Institutes of Health.

* To whom correspondence should be addressed. Phone: (858) 784-2223; fax: (858) 784-9822; e-mail: dyson@scripps.edu.

[‡] Present address: AMRAD Operations, Private Box 29, Richmond, Victoria 3121 Australia.

[§] Present address: Biotechnology Research Institute, National Research Council Canada, 6100 Royalmount Avenue, Montreal Quebec, H4P 2R2 Canada.

10.1021/bi001210r CCC: $19.00
Published on Web 10/07/2000

Xanthomonas (Pseudomonas) maltophilia (*10*), *Serratia marcescens* (*11*), and *Bacteroides fragilis* (*12*). Most cause postsurgical suppurative infections in humans, especially in those with weak immune response systems (*13*). Metallo-β-lactamases tend to be monomeric, except for the enzyme from *Stenotrophomonas maltophilia*, which is tetrameric (*14*). The metallo-β-lactamase from *B. fragilis* has been deemed the most problematic of all the β-lactamases studied thus far due to its high turnover (k_{cat}) and specificity (k_{cat}/K_m) exhibited against a broad range of clinical agents (*15*). Moreover, evidence is mounting to show that metallo-β-lactamase genes are being passed to other bacterial strains by plasmid (*3*) and integron-borne (*4*) transfer pathways. Therefore, the antibiotic resistance conferred through the production of metallo-β-lactamase will likely appear in more types of, and potentially more aggressive, bacterial strains.

Two essentially identical X-ray crystal structures of the metallo-β-lactamase from *B. fragilis* have been published (*15*, *16*). The overall structure consists of a four-layered $\alpha\beta/\beta\alpha$ motif, which, at present, is unique to the metallo-β-lactamases (*14*). The enzyme active site resides at one end of the β-sandwich and contains a binuclear zinc site. One zinc ion is coordinated to three histidine residues (His99 Nϵ, His101 Nδ, and His162 Nϵ) and a single water molecule, while the second zinc ion is coordinated with three residues (Asp103 Oδ2, Cys 181 Sγ, and His223 Nϵ) and two water molecules. One water molecule is coordinated (bridged) by both zinc ions and is thought to exist in hydroxide form. Recent kinetic and mechanistic studies of the enzyme (*17*) have suggested that upon binding, the carbonyl moiety of the β-lactam is activated for hydrolysis through polarization by one of the zinc ions followed by a *re*-face nucleophilic attack of the shared hydroxide to form an acyl−enzyme intermediate. Breakdown and release of the intermediate is then thought to occur in a rate-limiting step and appears to involve a proton transfer.

Flanking the enzyme active site at the edge of the β-sandwich reside two extended loop regions. The major loop (residues 43 through 54) constitutes a beta-sheet "flap", while the minor loop (residues 188 through 195) resides roughly opposite the flap centered about the binuclear zinc site. Crystallographic temperature factors, as well as the absence of electron density at the apex of the flap for one crystal structure (*16*) (disordered residues Gly48 and Trp49), are strong indications of polypeptide chain flexibility for this region of the protein. Crystallographic data for the corresponding loops of the similar metallo-β-lactamase from *Bacillus cereus* (*18*) and for the tetrameric L1 metallo-β-lactamase from *Stenotrophomonas maltophilia* (*14*) also suggest flexibility in these regions. This apparent conservation of flexibility in the vicinity of the active site may, in part, be critical for the function of many metallo-β-lactamases.

A recent study (*19*) showed that the interaction of the metallo-β-lactamase from *B. fragilis* with a tight binding inhibitor (SB225666) resulted in significant NMR chemical shift perturbations of backbone amides of these flanking loop regions. In addition, indole NH resonances of tryptophans 49 and 100 were observed to shift significantly upon inhibitor binding. ^{15}N-^{1}H heteronuclear NOEs for backbone amides that constitute the major flap increase somewhat upon inhibitor binding indicating a slight reduction in flap mobility

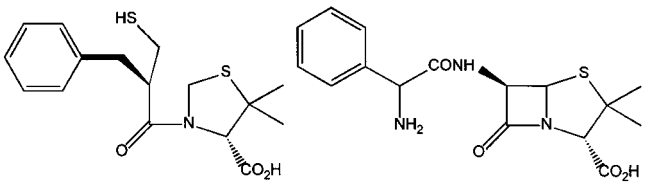

FIGURE 1: Structural comparison of (a) SB225666 and (b) ampicillin.

on the pico- to nanosecond time scale. The tryptophan side chain indoles exhibit high heteronuclear NOEs, which change little upon inhibitor binding. The exception is W49, which is highly mobile in the free form but becomes noticeably restricted upon addition of inhibitor.

These and other investigations strongly suggest that polypeptide chain dynamics in the vicinity of the lactamase active site may play a critical role in the binding of substrates and/or stabilization of intermediates in its catalytic mechanism. In this paper, we examine in detail the backbone and tryptophan indole dynamics of this metallo-β-lactamase in the presence and absence of a tight-binding inhibitor (SB225666) to assess the role of polypeptide chain dynamics in the catalytic mechanism of this enzyme.

MATERIALS AND METHODS

Sample Preparation. ^{15}N-labeled metallo-β-lactamase samples were prepared according to previously described methods (*19*). NMR samples were suspended in 10 mM HEPES, 100 μM $ZnCl_2$, and 0.01% NaN_3 (pH 7.0) (5% D_2O). Metallo-β-lactamase sample activity was assayed using nitrocefin (Oxoid) and yielded the following kinetic values: $k_{cat} = 214$ s^{-1}, $K_m = 13.8$ μM, and $V_{max} = 1.3$ μM s^{-1}, consistent with previously published data (*20*).

Samples of the proprietary inhibitor 3-[2′-(*S*)-benzyl-3′-mercaptopropanoyl]-4-(*S*)-carboxy-5,5-dimethylthiazolidine (SB225666) (Figure 1), were obtained from SmithKline Beecham. NMR samples of the lactamase bound to SB225666 were prepared by the addition of the inhibitor dissolved in dimethyl sulfoxide (DMSO) under anaerobic conditions to a final concentration of 6 mM and 3% DMSO. The final concentration of the lactamase was 125 μM for all NMR samples. The use of such dilute protein samples was necessitated by the observed aggregation of the protein at concentrations above 250 μM (unpublished data).

NMR Spectroscopy. NMR spectra were acquired at 295 K on a Bruker DRX-600 spectrometer equipped with an 8-mm inverse-detected triple-resonance single axis gradient probe from Nalorac (Martinez, CA). ^{15}N R_1 and R_2 relaxation data for both free and inhibitor-bound lactamase samples were acquired according to Farrow et al. (*21*, *22*). For the determination of R_1 relaxation time constants, 13 total data sets were collected at relaxation delay times of 10, 200, 500, 800, 1000, 1100, 1200, 1400, 1800, and 2200 ms. For the assessment of peak height uncertainties, duplicate experiments were conducted at 10, 500, and 1000 ms. For the determination of R_2 time constants, 13 data sets were also collected at delay times of 6, 22, 42, 50, 62, 90, 110, 150, and 202 ms with duplicate experiments being acquired at 6, 62, and 110 ms. R_1 and R_2 spectra were recorded as 256 × 1024 complex data points with 16 transients/point. Spectral widths were 1580 and 9615 Hz along the ^{15}N and ^{1}H dimensions, respectively. A 2.5-s recycle delay was used for

all R_1 and R_2 experiments. Heteronuclear NOE spectra were recorded as 128 × 1024 complex data points with 128 transients/point. Spectral widths for the ^{15}N and ^{1}H were identical as described above. Heteronuclear NOE values were determined from the ratio of peak intensity in the absence and presence of proton saturation (*23*). Saturation was achieved by use of a train of 120° pulses separated by 5 ms for a total irradiation time of 3 s (*22*, *24*). A 4-s recycle delay was employed for all heteronuclear NOE experiments. For the determination of peak height uncertainties, four identical saturated/unsaturated experiments were acquired. Reduction of the intense water resonance in the presence of severe radiation damping was accomplished by use of a 2.0-ms water-selective soft pulse in conjunction with a water-selective inversion pulse train (3-9-19 WATERGATE) (*25*).

Spectra were processed using either Felix 95.0 (MSI) or NMRPipe/NMRDraw (*26*) and analyzed with either Felix 95.0 or NMRView (*27*). Data sets were zero filled and apodized with exponential, cosine-squared, or Lorenzian-to-Gausian window functions. Linear prediction was used to extend the ^{15}N indirect dimension thereby improving digital resolution. Proton chemical shifts were referenced to external 2,2-(dimethylsilyl)propanesulfonic acid (DSS) and ^{15}N chemical shifts were referenced indirectly to DSS. NMR probe temperature was carefully calibrated using neat methanol (*28*). Subsequent analyses used backbone amide and tryptophan indole NH resonance assignments previously determined for both the free and the inhibitor-bound forms of the protein by Scrofani et al. (*19*, *29*). Overlapped resonances were eliminated from further analyses.

R_1, R_2, and heteronuclear NOE values were determined from resonance peak heights as described by Stone et al. (*30*, *31*) using in-house programs and/or programs developed by Dr. A. G. Palmer (*32*). Uncertainties in heteronuclear NOE values were calculated as described by Nicholson et al. (*33*). To rule out any effect of the addition of DMSO on the internal mobility of the enzyme (through partial denaturation or dimerization), an inhibitor-free protein sample containing 3% DMSO was prepared, and R_1, R_2, and heteronuclear NOE measurements were made in the same way as for the DMSO-free sample. The relaxation data for this sample showed negligible difference in the backbone or tryptophan indole relaxation behavior relative to the inhibitor-free sample.

Estimation of τ_m and the Analysis of Isotropic versus Axially Symmetric Diffusion. In the case in which the overall rotational correlation time, τ_m, is greater than 1 ns, the effective correlation time, τ_e, is less than 100 ps, and R_2 is not significantly lengthened by chemical exchange, the ratio of R_2 to R_1 can be used to derive an approximation for τ_m (*34*−*36*). Residues with heteronuclear NOEs less than 0.65 or residues with a R_2/R_1 ratio that lay outside one standard deviation of the calculated R_2/R_1 average were eliminated from the final estimation of τ_m.

To distinguish between isotropic and axially symmetric diffusion models, hydrodynamic and inertia calculations were performed on the 1bmi X-ray crystal structure coordinates (*15*) using an in-house program, MASH (written by Ishwar Radhakrishnan) which employs the HYDRO suite of algorithms developed by Garcia de la Torre and Bloomfield (*37*). Each residue was modeled as a single bead centered on the C_α atom. The viscosity was that of water at 295 K. The hydration shell was optimized by minimizing the error function $\Gamma = \Sigma\eta_i^2$, where η_i^2 compares the goodness-of-fit of the calculated local diffusion coefficients [$D_{i(pred)}$] with the experimentally determined local diffusion coefficient [$D_{i(exp)}$] obtained from R_2/R_1 ratios. Prior to these calculations, hydrogen atoms were added to the crystal structure using the preparatory program PROTONATE, which is a module of the AMBER suite of programs (*38*). Structure coordinates within the frame of reference of the diffusion tensor were output along with rotational diffusion coefficients (D_{zz}, D_{yy}, and D_{xx}), as well as local θ and ϕ angles for NH bond vectors (with respect to the principal axis of the diffusion tensor). For both free and inhibitor-bound data sets, plots of R_2/R_1 versus $(3\cos^2\theta - 1)/2$ (where θ is derived from the output of MASH) were examined to determine the extent of axial or anisotropic rotational diffusion (*39*, *40*). F-statistical testing was used to ascertain the statistical significance of isotropic versus axially symmetric diffusion models using the programs "pdbinertia" and "quadric_diffusion" (*32*). Again, residues with NOEs less than 0.65 or residues with a R_2/R_1 ratio that lay outside one standard deviation of the calculated R_2/R_1 average were excluded from these analyses. Because no X-ray crystal structures of this metallo-β-lactamase bound to SB225666 have been published, we have used the same X-ray structure coordinates used for the free, unbound form of the protein to evaluate the overall rotation of the protein in its inhibitor-bound form. We have previously determined that binding of SB225666 results in only slight structural changes localized to the active site region (*19*). Therefore, we have assumed that the binding of the inhibitor does not substantially affect the general structure of the protein, and by consequence, its overall rotation.

Model-Free Analyses. Analyses of the derived relaxation rate parameters and heteronuclear NOE values was performed according to the model-free and extended model-free formalisms (*35*, *41*, *42*) by use of ModelFree 4.10 (*43*). Model selection and statistical testing of models were performed according to Mandel et al. (*44*). The goodness-of-fit between the experimentally derived relaxation data and each of the five motional models considered was determined by comparison of the minimum value of the χ^2 function at the 95% confidence limit of the χ^2 probability distribution determined from 400 Monte Carlo simulations. In the case in which spins satisfied the χ^2 function at the 95% confidence level (for more complicated models 2 or 3) but did not satisfy F-testing ($\alpha = 0.15$ critical level), the simpler model 1 was assigned by default. Fits that did not strictly satisfy 95% χ^2-statistic levels for models 1 through 3 were considered to be inadequately fit by any of these motional models. However, this statistical treatment cannot be used in the assignment of models 4 or 5 (*36*). Therefore, assignment of models 4 and 5 was accomplished using methods as described by Mandel et al. (*44*). Particular care was taken for assignment of residues to model 5 as selection of this model can result in false characterization of motion due to anisotropic tumbling (*45*). Therefore, model 5 was assigned only when the sum-squared error for the spin under consideration was zero and the next best-fit model for the spin (usually model 2) had a large 95% χ^2-statistic value (generally greater than 40). The relaxation data for the tryptophan side-chain indoles were analyzed in an identical manner to those of the backbone amides. In this case,

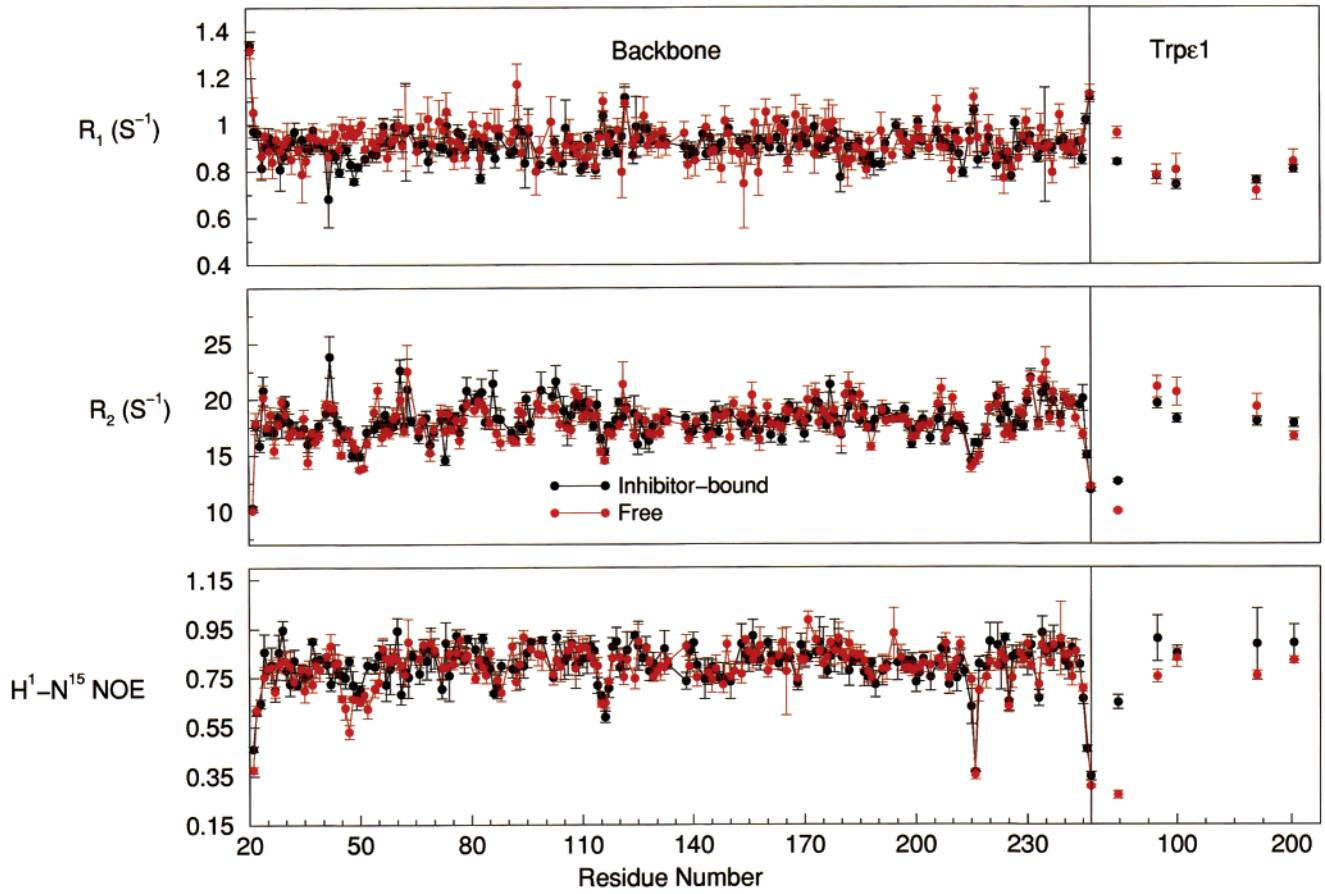

FIGURE 2: ^{15}N backbone amide relaxation parameters measured for the free (red) and inhibitor-bound (black) metallo-β-lactamase versus residue number. Shown from top to bottom are longitudinal relaxation rates (R_1), transverse relaxation rates (R_2), and ^{1}H-^{15}N heteronuclear NOE values, respectively. The average heteronuclear NOE value for residues that constitute the major flap (44−54) is 0.67 for the free form and 0.76 for the inhibitor-bound form of the protein. Values for the tryptophan indole NHs (Trpϵ1) are shown as separate graphs to the right of the figure. Trp49 is highly mobile in the free form of the protein with a ^{1}H-^{15}N heteronuclear NOE of 0.28. However, Trp49 for the inhibitor-bound protein exhibits significantly less mobility with a ^{1}H-^{15}N heteronuclear NOE of 0.60.

however, a chemical shift anisotropy (CSA) of −89 ppm was assumed for the model-free analysis (*46*).

The initial estimates of τ_m and D_{rat} for each of the free and inhibitor-bound data sets were used in the first round of model selection. The internal motional parameters for the selected models for each NH and Nϵ1 vector were then simultaneously optimized with the overall diffusion tensor. Rounds of fixed model selection employing the newly optimized diffusion tensor and reoptimization were conducted until consistent model selection and a convergence of the overall diffusion tensor was achieved.

RESULTS

Sequential NH backbone and Nϵ1 tryptophan indole resonance assignments of the metallo-β-lactamase from *B. fragilis* in its free and SB225666-bound forms have previously been determined and have been used for the present study (*19*, *29*). All five tryptophan indole resonances for both the free and inhibitor-bound protein samples were sufficiently resolved for accurate peak height determination. For the free protein, 179 of 218 amide resonances were sufficiently resolved for accurate peak height measurement. For the inhibitor-bound protein, 185 of 218 amide resonances were resolvable. In each instance, this represents approximately 83% of all residues excluding prolines 53, 71, 97, 134, 136, 152, 172, 214, 221, and 249.

Relaxation Parameters. Figure 2 summarizes the derived relaxation data for the free and inhibitor-bound metallo-β-lactamase. Backbone R_1, R_2, and heteronuclear NOE values for the free and inhibitor-bound forms of the protein correlate quite well. Although there do not appear to be any major differences in R_2, noticeable decreases in R_1 and slight increases in heteronuclear NOEs can be observed for residues that constitute the major flap (residues 43 through 54) upon binding of SB225666. Data for two short secondary loops, 115−117 and 214−217, show remarkable similarity for both data sets as do residues of the N and C termini. Data for residues of the minor active site loop, which resides roughly opposite the major flap (residues 184 through 193), are also quite similar for both data sets. The exception is 188, which possesses a somewhat shorter R_2 value for the free protein. Data for the tryptophan side chains (shown as separate graphs to the right of the figure) indicate that the relaxation parameters vary little between free and bound forms of the protein. The exception is Trp49, which shows significant changes in R_1, R_2, and heteronuclear NOE upon inhibitor binding.

Estimation of τ_m and Analysis of Isotropic versus Axially Symmetric Diffusion. NMR samples prepared according to the protocol detailed by Scrofani et al. (*19*) showed no evidence for aggregation or dimerization by gel-filtration or SDS−PAGE for sample concentrations ranging from

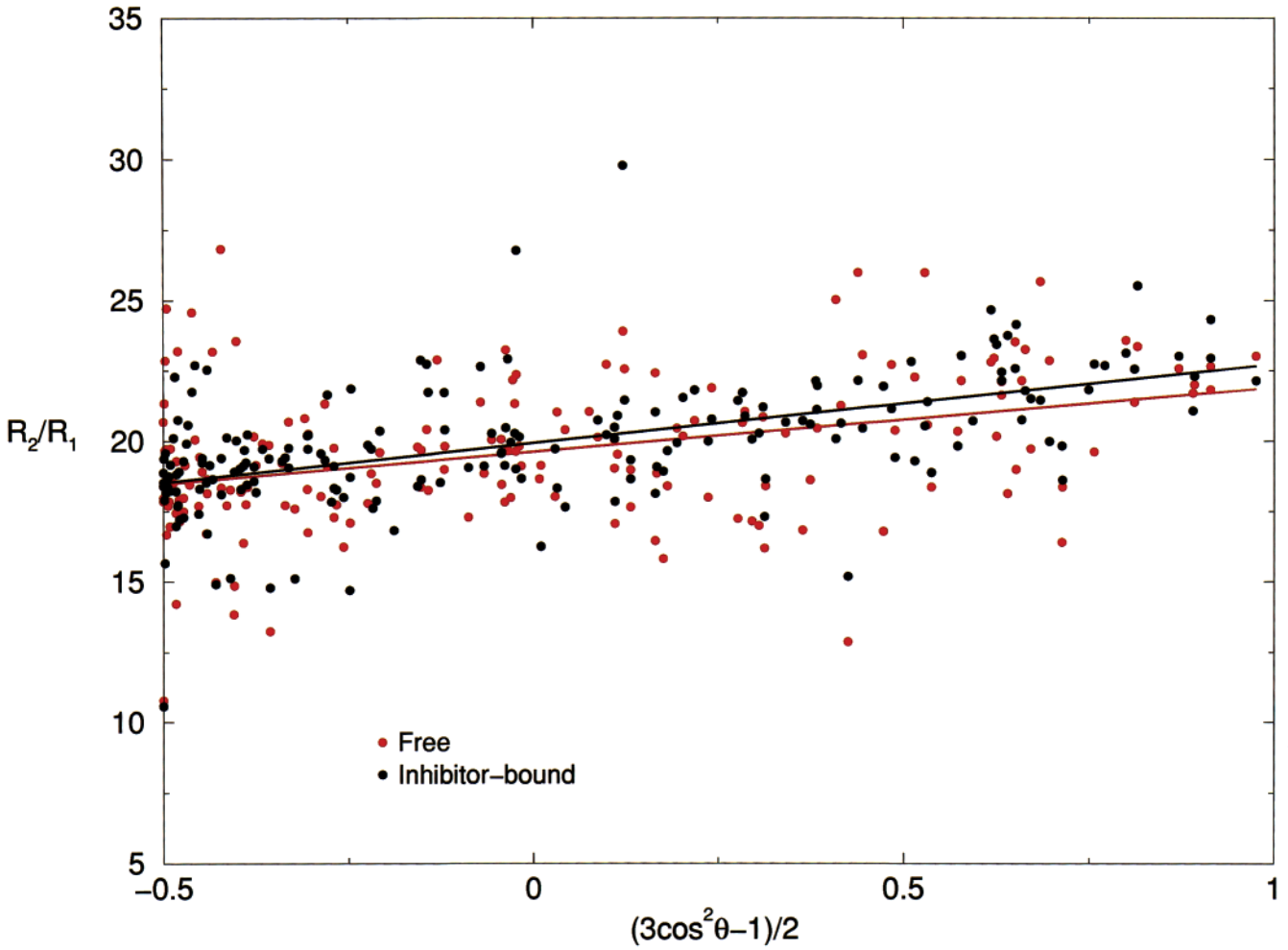

FIGURE 3: Plots of the experimental R_2/R_1 data for the free (red) and bound (black) forms of the protein versus $(3\cos^2\theta - 1)/2$. θ represents the local angles for NH bond vectors with respect to the principal axis of the diffusion tensor (derived from the output of MASH). The slopes of the linear least-squares fit to the data were 2.29 ± 0.42 (correlation coefficient = 0.38) and 2.81 ± 0.32 (correlation coefficient = 0.54) for the free and inhibitor-bound data sets, respectively.

125 μM to 1.3 mM. However, some evidence for aggregation for samples at 250 μM was observed principally through R_2 data, as well as the subsequent determination of anomalous overall rotational correlation times for free and inhibitor-bound samples (S. D. Scrofani and H. J. Dyson, unpublished). A reduction in sample concentration to 125 μM, however, indicated a monodisperse monomeric sample as demonstrated by R_2 data, as well as resultant rotational correlation times of 14.0 ± 0.8 and 14.1 ± 0.7 ns for free and inhibitor-bound protein, respectively.

Hydrodynamic and inertia calculations (M. J. Osborne and P. E. Wright, unpublished) using the 1bmi X-ray crystal structure (*15*) were used to judge the nature of the overall diffusion of the protein in solution (isotropic versus axially symmetric). Plots of backbone R_2/R_1 values versus $(3\cos^2\theta - 1)/2$ [the spherical harmonic function, $Y_2^0(\theta)$] are shown in Figure 3. These results demonstrate a clear angular dependence of the experimental R_2/R_1 data, indicating that the protein does not rotate isotropically but rather axially or anisotropically. This is shown by the nonzero slope of the derived linear least-squares fit to the data (2.29 ± 0.42 and 2.81 ± 0.32 for the free and inhibitor-bound protein, respectively). Statistical F-testing employing the program quadric_diffusion (*32*) demonstrated that the more complicated anisotropic diffusion model did not significantly improve the description of the overall diffusion of the protein, as compared to the axially symmetric diffusion model (F = 0.38). Therefore, an axially symmetric model of diffusion was assumed for subsequent model-free analyses of the free and inhibitor-bound relaxation data sets. The overall rotational correlation time τ_m was 14.0 ns, with an estimated axially symmetric diffusion coefficient D_{rat} of 1.21(derived from the output of MASH, where $D_{rat} = D_{||}/D_{\perp} = D_{zz}/[(D_{xx} + D_{yy})/2)]$.

Model-Free Results. The results of the model-free analyses are summarized in Figure 4. Six rounds of model selection and optimization were conducted for the free and inhibitor-bound relaxation data sets until consistent model selection and convergence of the overall diffusion tensor was observed. Diffusion tensors converged to similar values of τ_m = 13.96 ns, D_{rat} = 1.25, $\theta = -65.4°$, and ϕ = 29.9, and τ_m = 13.96 ns, D_{rat} = 1.18, $\theta = -59.0°$, and ϕ = 38.5 for the free and bound data sets, respectively. For the free protein, 168 of 179 resolvable backbone amides were fit to one of the five motional models considered. Seventy-four percent of residues were fit to model 1 (S^2), and 6% were fit to model 2 (S^2, τ_e). Residues 156 and 185 were fit to model 3 (S^2, R_{ex}) while only one residue, 207, was fit to model 4 (S^2, τ_e, and R_{ex}). Fifteen residues were fit to model 5 (S_s^2, S_f^2, and τ_e). These included two residues of the N-terminus (21 and 25), two

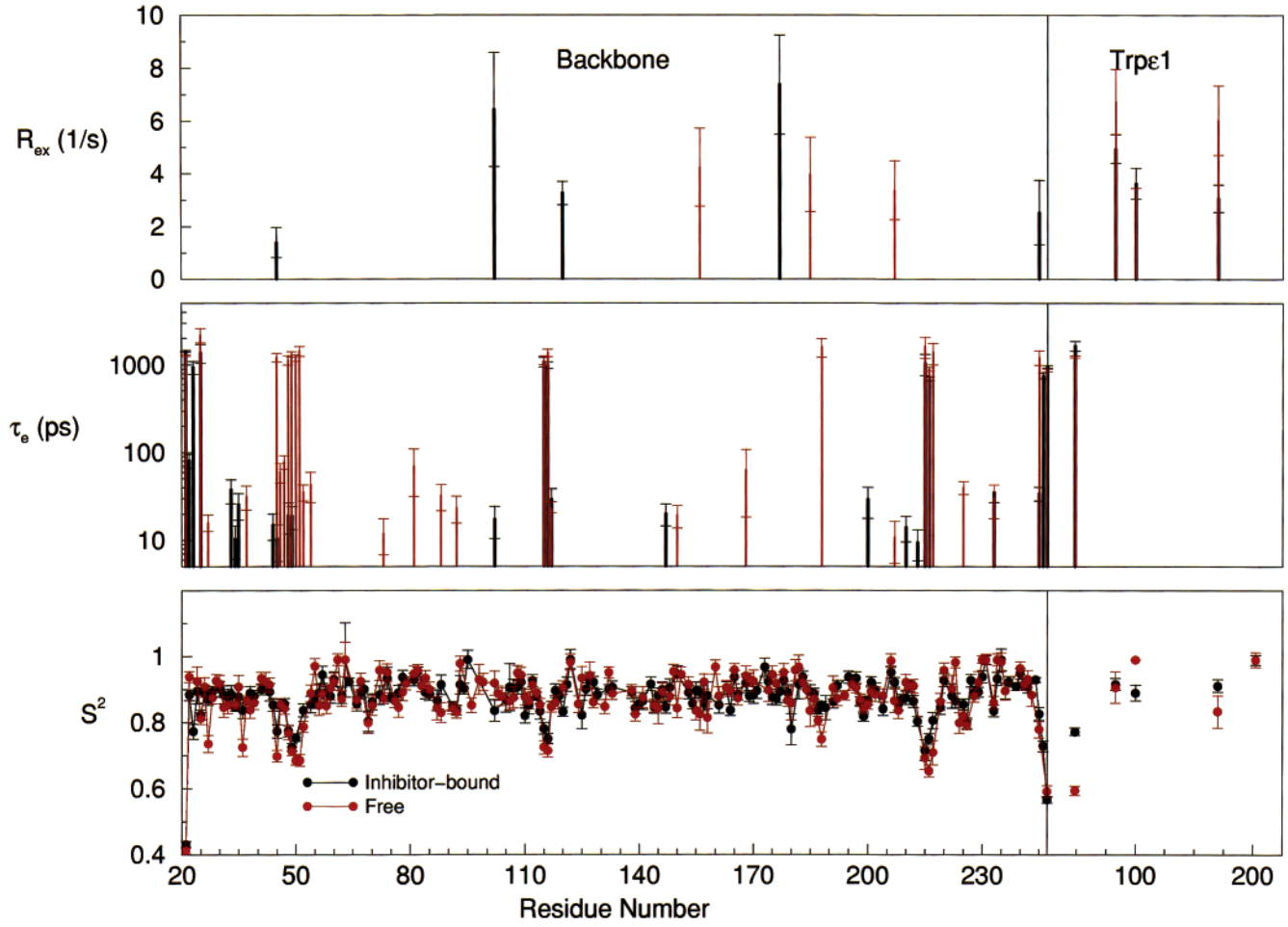

FIGURE 4: Plots of the model-free parameters versus residue number for the metallo-β-lactamase in the presence (black circles and bars) and absence (red circles and bars) of SB225666. Shown from top to bottom are R_{ex}, τ_e, and S^2, respectively. Parameters for the tryptophan indoles are shown in separate plots to the right of the figure. Effective correlation times (τ_e) for the free protein (center plot) demonstrate nanosecond time scale motions for residues that constitute the major flap (44−54) as well as for residue 188 of the minor active site loop. These relatively long correlation times are absent for the same residues of the inhibitor-bound form of the protein.

residues of the C-terminus (245 and 247), and five residues of two short loops (115, 116, and 215−217). Five backbone amides of the major flap were fit to model 5 for the free protein. These included residues 45 and 48−51. Furthermore, residues 46, 47, 52, and 54 of the flap were fit to model 2. For the inhibitor-bound protein, 169 of 185 resolvable backbone amides were fit to models 1 through 5. Seventy-seven percent were fit to model 1, and 7% were fit to model 2. Three residues (95, 120, and 177) were fit to model 3, while residues 45, 102, and 245 were fit to model 4. For the inhibitor bound protein, nine residues were fit to model 5. These included three residues of the N-terminus (21, 23, and 25), two residues of the C-terminus (246 and 247), and four residues of the two short loops (115, 116, and 215−216). In contrast to the results of model selection for the free protein, there were no residues of the major flap that fit to model 5. Residues 44, 49, and 50, however, were fit to model 2.

The results of the model-free analyses for the tryptophan indoles of the free and inhibitor-bound proteins are also shown to the right of Figure 4. For both samples, tryptophan 202 was fit to model 1, tryptophans 83, 100, and 183 were fit to model 3, and tryptophan 49 was fit to model 5.

Inspection of the figure reveals that the derived order parameters (S^2) for the backbone of the free and bound forms of the protein are remarkably similar. S^2 values for residues of loops 115−117 and 214−217 correlate well, as do values for the N and C termini. Data for the major flap show a slight reduction in S^2 upon binding of SB225666, as do S^2 values for the minor active site loop. Data for the tryptophans, also shown as separate graphs to the right of the figure, indicate a similarity in S^2 values for the side chain indoles. Again, the exception is tryptophan 49. For the free form of the protein, the indole has a somewhat reduced S^2 value of 0.58. However, upon binding of SB225666, the order parameter substantially increases to a value of approximately 0.75.

Analysis of the time scales of motion for the two forms of the protein reveal that effective correlation times for residues of loops 115−117, 215−217, and residues of the N and C termini correlate well with observed τ_e values of approximately 1 ns. More significant are changes that occur to the time scales of motion for the major flap and minor active site loop upon binding of the inhibitor. For the free form of the protein, residue 45 and residues 48−51 have effective correlation times of approximately 1.3 ns. These relatively long correlation times are completely absent for the inhibitor-bound protein. Furthermore, residue 188 of the minor active site loop has an effective correlation time of approximately 1.6 ns. Again, this relatively long correlation time is absent for the same residue in the inhibitor-bound

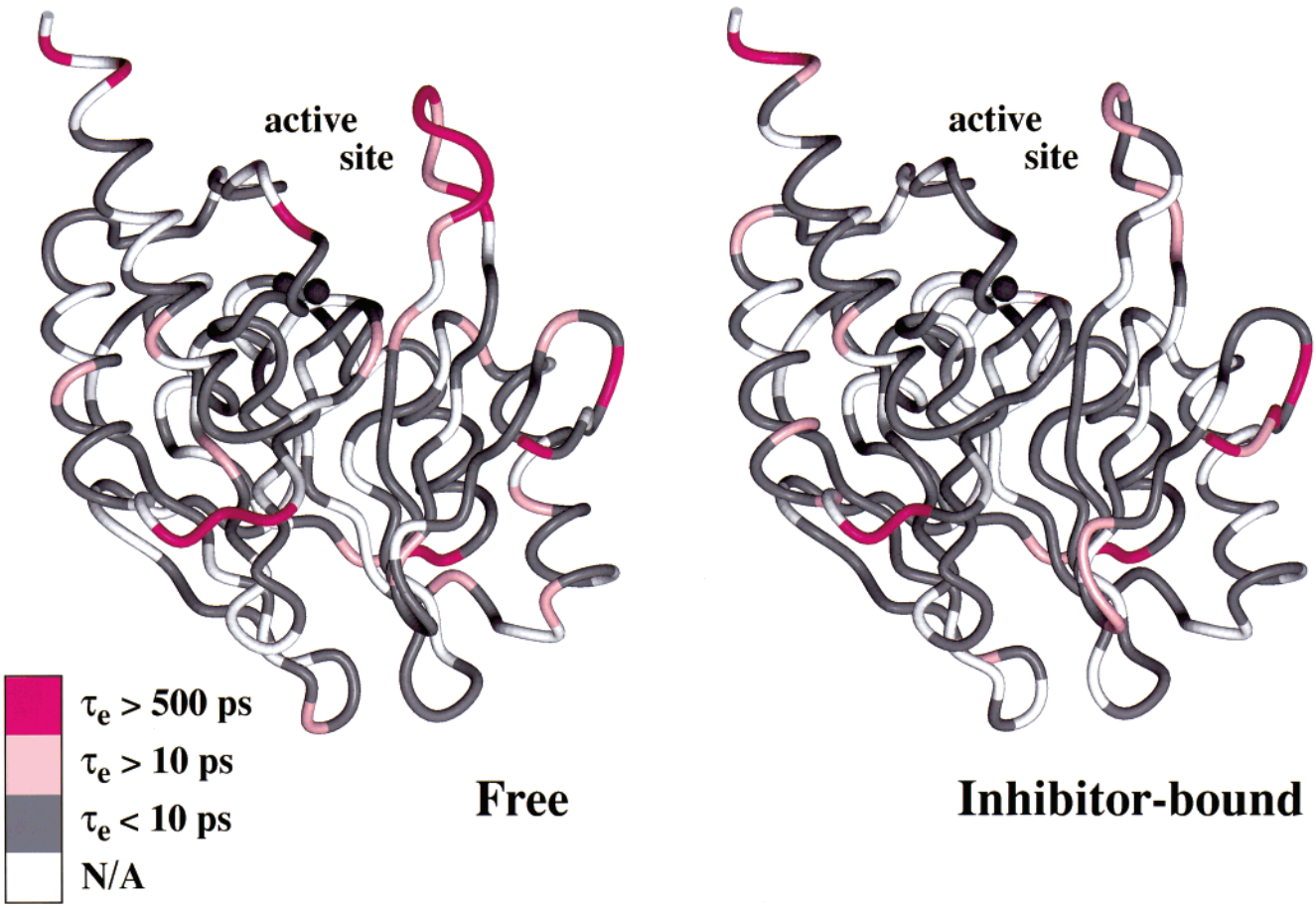

FIGURE 5: Effective correlation times for internal motion mapped onto the X-ray crystal structure (*15*) for the free and inhibitor-bound forms of the protein. Long correlation times (τ_e > 500 ps) are shown in hot pink (model 5), while intermediate correlation times (10 > τ_e > 500 ps) are shown in light pink (model 2). Residues with fast internal motions (τ_e < 10 ps) are shown in gray. Residues that were not fit any model or residues for which relaxation data was unobtainable due to spectral overlap are shown in white. Inspection of the figure reveals that differences in time scales of motion are localized to the active site region. For the major flap, the average τ_e is 720 ps, while residue 188 of the minor loop possesses a τ_e of 1600 ps. For the same residues of the inhibitor bound protein, only residues 44, 45, 48, and 49 (all model 2) possess a small average τ_e of 15.8 ps.

form of the protein. Data for tryptophan 49 indicate that the side chain has an effective correlation time of approximately 1 ns for the free protein, which increases slightly to approximately 1.5 ns upon binding of the inhibitor. While some exchange terms (R_{ex}) are present for a number of residues, there is no correlation for data of the backbone amides of the free and inhibitor-bound protein. Data for tryptophans 83, 100, 183, and 202, however, do correlate well, each requiring a similar R_{ex} value.

DISCUSSION

Our relaxation data, and subsequent model-free analyses of these data, reveal that the overall structure of the metallo-β-lactamase is relatively rigid, except for residues of the N and C termini, residues of the two short secondary loops, and for residues that constitute the major flap at the active site and the minor active-site loop. Interestingly, the flexibility of the two active site components, the major flap and the minor loop, is not inordinately greater than that of the other loops of the protein. Indeed, backbone motions on the picosecond time scale (indicated by S^2 values) were found to be similar throughout the protein in the presence and absence of the inhibitor. However, marked changes in the time scales of motion are observed for the flap and minor loop upon binding of SB225666 (Figure 5). The free protein shows relatively long (nanosecond) effective correlation times (τ_e) of residues of the flap; these are completely damped upon binding of the inhibitor. Further, the slow motions (τ_e) of residue 188 of the minor active site loop also disappear upon binding of the inhibitor.

These data suggest that upon binding, the flap, and to a lesser extent the minor active site loop, collapses down around the substrate, effectively locking it in an induced-fit fashion. This tightening of the active site region about the substrate may then promote catalysis in the Michaelis complex through orientation of substrates within the active site or stabilization of intermediates that define the catalytic mechanism.

Changes in the dynamics of the tryptophan at the apex of the flap (Trp49) that occur upon binding of the inhibitor suggest a specific role for this side chain in the binding of substrates. In the free form of the protein, the indole possesses a reduced heteronuclear NOE (Figure 2). Upon binding of SB225666, the heteronuclear NOE increases substantially, indicating a reduced flexibility of the side chain on a pico- to nanosecond time scale. The model-free results for this tryptophan are consistent with a significant reduction in side chain flexibility as well. It is not yet clear which factors are responsible for the reduction of the flexibility of the indole. It is possible that the tryptophan interacts with

the substrate (e.g., through the thiazoline moiety) and is mainly responsible for the pinning down of the flap against the inhibitor. Alternatively, the flap could be pinned down against the inhibitor through interactions that do not involve the tryptophan side chain, and thus, the reduction in flexibility of the indole is a fortuitous consequence of such interactions. For example, as suggested by Herzberg and co-workers (*16*), residues 44, 46, 52, and 72 on the active site side of the flap may form a hydrophobic pocket into which the β-side chain of many lactam-based antibiotics may be well-accommodated. It is possible that such hydrophobic protein−substrate interactions would result in a decrease in flexibility of the entire flap, including the indole at its apex. It is also plausible that a combination of nonspecific hydrophobic and specific side chain protein−substrate interactions results in the observed tightening of the binding pocket upon incorporation of substrates. We are presently investigating the nature of such interactions to better characterize the exact role of the tryptophan side chain in the binding of substrates.

In 1998, Fitzgerald and co-workers (*47*) reported the unanticipated inhibition of this lactamase by 4-morpholineethanesulfonic acid (MES). Shortly thereafter, Toney et al. (*48*) reported antibiotic sensitization of the metallo-β-lactamase from *B. fragilis* using biphenyl tetrazoles as inhibitors. In each instance, X-ray crystal structures of the enzyme bound to either MES or to biphenyl tetrazole L-159,061 localized the inhibitors within the enzyme binding site. However, there was no correlation to how the inhibitors were oriented, each taking up a different position within the binding site. In addition, the relative position of the major flap was shown to bend slightly toward the substrates relative to the unbound form of the enzyme. However, the extent to which the flap closed down upon the inhibitors was variable among structures. Our results suggest that polypeptide chain dynamics of the flap and minor active site loop gives rise to a plastic binding site that can mold around substrates of varying size and composition. This plasticity is a necessary and underlying determinant for the full catalytic function of the enzyme.

One of the major concerns in the proliferation of the metallo-β-lactamases is the broad substrate specificity of this enzyme, which allows bacteria to resist whole classes of antibiotics such as penicillins and cephalosporins. Derivatization of the antibiotic in an effort to combat resistance will clearly be rather ineffective for bacteria that harbor metallo-β-lactamases. An essential component for the broad substrate specificity of the metallo-β-lactamase from *B. fragilis* and similar antibiotic-resistant organisms is the presence of a dynamic binding site, which is capable of the tight binding of structurally diverse substrates.

ACKNOWLEDGMENT

We thank Drs. John Chung and Gerard Kroon for assistance with acquisition and analysis of NMR data, Linda Tennant for expert technical assistance, and Drs. Brendan Duggan, Maria Yamout, and Eduardo Zaborowski for helpful discussions. We acknowledge productive collaboration in this work with Drs. Stephen Benkovic and David Case.

REFERENCES

1. Knowles, J. R. (1985) *Acc. Chem. Res. 18*, 97−104.
2. Bandoh, K., Watanabe, K., Muto, Y., Tanaka, Y., Kato, N., and Ueno, K. (1992) *J. Antibiot. (Tokyo) 45*, 542−547.
3. Ito, H., Arakawa, Y., Ohsuka, S., Wacharotayankun, R., Kato, N., and Ohta, M. (1995) *Antimicrob. Agents Chemother. 39*, 824−829.
4. Senda, K., Arakawa, Y., Ichiyama, S., Nakashima, K., Ito, H., Ohsuka, S., Shimokata, K., Kato, N., and Ohta, M. (1996) *J. Clin. Microbiol. 34*, 2909−2913.
5. Hughes, J. M., and Tenover, F. C. (1997) *Clin. Infect. Dis. 24*, S131−S135.
6. Bush, K. (1989) *Antimicrob. Agents Chemother. 33*, 264−271.
7. Levy, S. B., and Nelson, M. (1998) *Adv. Exp. Med. Biol. 456*, 17−25.
8. Bush, K. (1989) *Antimicrob. Agents Chemother. 33*, 271−276.
9. Bush, K., Jacoby, G. A., and Medeiros, A. A. (1995) *Antimicrob. Agents Chemother. 39*, 1211−1233.
10. Saino, Y., Kobayashi, F., Inoue, M., and Mitsuhashi, S. (1982) *Antimicrob. Agents Chemother. 22*, 564−570.
11. Yang, Y., Wu, P., and Livermore, D. M. (1990) *Antimicrob. Agents Chemother. 34*, 755−758.
12. Cuchural, G. J., Malamy, M. H., and Tally, F. P. (1986) *Antimicrob. Agents Chemother. 30*, 645−648.
13. Rasmussen, B. A., Bush, K., and Tally, F. P. (1993) *Clin. Infect. Dis. 16* Suppl. 4, S390−S400.
14. Ullah, J. H., Walsh, T. R., Taylor, I. A., Emery, D. C., Verma, C. S., Gamblin, S. J., and Spencer, J. (1998) *J. Mol. Biol. 284*, 125−136.
15. Carfi, A., Duée, E., Paul-Soto, R., Galleni, M., Frère, J.-M., and Dideberg, O. (1998) *Acta Crystallogr. Sect. D 54*, 47−57.
16. Concha, N. O., Rasmussen, B. A., Bush, K., and Herzberg, O. (1996) *Structure 4*, 823−836.
17. Wang, Z. G., and Benkovic, S. J. (1998) *J. Biol. Chem. 273*, 22402−22408.
18. Carfi, A., Pares, S., Duée, E., Galleni, M., Duez, C., Frére, J. M., and Dideberg, O. (1995) *EMBO J. 14*, 4914−4921.
19. Scrofani, S. D. B., Chung, J., Huntley, J. J. A., Benkovic, S. J., Wright, P. E., and Dyson, H. J. (1999) *Biochemistry 38*, 14507−14514.
20. Rasmussen, B. A., Gluzman, Y., and Tally, F. P. (1990) *Antimicrob. Agents Chemother. 34*, 1590−1592.
21. Farrow, N. A., Muhandiram, R., Singer, A. U., Pascal, S. M., Kay, C. M., Gish, G., Shoelson, S. E., Pawson, T., Forman-Kay, J. D., and Kay, L. E. (1994) *Biochemistry 33*, 5984−6003.
22. Farrow, N. A., Zhang, O., Forman-Kay, J. D., and Kay, L. E. (1995) *Biochemistry 34*, 868−878.
23. Noggle, J. H., and Schirmer, R. E. (1971) in *The Nuclear Overhauser Effect. Chemical Applications*, Academic Press, New York.
24. Markley, J. L., Horseley, W. J., and Klein, M. P. (1971) *J. Chem. Phys. 55*, 3604−3605.
25. Sklenar, V., Piotto, M., Leppik, R., and Saudek, V. (1993) *J. Magn. Reson. 102*, 241−245.
26. Delaglio, F., Grzesiek, S., Vuister, G. W., Guang, Z., Pfeifer, J., and Bax, A. (1995) *J. Biomol. NMR 6*, 277−293.
27. Johnson, B. A., and Blevins, R. A. (1994) *J. Chem. Phys. 29*, 1012−1014.
28. Van Geet, A. L. (1970) *Anal. Chem. 42*, 679−680.
29. Scrofani, S. D., Wright, P. E., and Dyson, H. J. (1998) *J. Biomol. NMR 12*, 201−202.
30. Stone, M. J., Chandrasekhar, K., Holmgren, A., Wright, P. E., and Dyson, H. J. (1993) *Biochemistry 32*, 426−435.
31. Stone, M. J., Fairbrother, W. J., Palmer, A. G. III, Reizer, J., Saier, M. H. Jr., and Wright, P. E. (1992) *Biochemistry 31*, 4394−4406.
32. Palmer, A. G., III (1996) http://cpmcnet.columbia.edu/dept/gsas/biochem/labs/palmer/software.html.
33. Nicholson, L. K., Kay, L. E., Baldisseri, D. M., Arango, J., Young, P. E., Bax, A., and Torchia, D. A. (1992) *Biochemistry 31*, 5253−5263.

34. Kay, L. E., Torchia, D. A., and Bax, A. (1989) *Biochemistry 28*, 8972−8979.
35. Clore, G. M., Driscoll, P. C., Wingfield, P. T., and Gronenborn, A. M. (1990) *Biochemistry 29*, 7387−7401.
36. Sari, N., Holden, M. J., Mayhew, M. P., Vilker, V. L., and Coxon, B. (1999) *Biochemistry 38*, 9862−9871.
37. Garcia de la Torre, J. G., and Bloomfield, V. A. (1981) *Q. Rev. Biophys. 14*, 81−139.
38. Pearlman, D. A., Case, D. A., Caldwell, J. W., Ross, W. S., Cheatham, T. E., III, Ferguson, D. M., Seibel, G. L., Singh, U. C., Weiner, P. K., and Kollman, P. A. (1995) in *AMBER 4.1*, University of California, San Francisco.
39. Lee, L. K., Rance, M., Chazin, W. J., and Palmer, A. G., III (1997) *J. Biomol. NMR 9*, 287−298.
40. Campos-Olivas, R., and Summers, M. F. (1999) *Biochemistry 38*, 10262−10271.
41. Lipari, G., and Szabo, A. (1982) *J. Am. Chem. Soc. 104*, 4546−4559.
42. Lipari, G., and Szabo, A. (1982) *J. Am. Chem. Soc. 104*, 4559−4570.
43. Palmer, A. G. III (2000) http://cpmcnet.columbia.edu/dept/gsas/biochem/labs/palmer/software.html.
44. Mandel, A. M., Akke, M., and Palmer, A. G., III (1995) *J. Mol. Biol. 246*, 144−163.
45. Phan, I. Q. H., Boyd, J., and Campbell, I. D. (1996) *J. Biomol. NMR 8*, 369−378.
46. Cross, T. A., and Opella, S. J. (1983) *J. Am. Chem. Soc. 105*, 306−308.
47. Fitzgerald, P. M., Wu, J. K., and Toney, J. H. (1998) *Biochemistry 37*, 6791−6800.
48. Toney, J. H., Fitzgerald, P. M. D., Grover-Sharma, N., Olson, S. H., May, W. J., Sundelof, J. G., Vanderwall, D. E., Cleary, K. A., Grant, S. K., Wu, J. K., Kozarich, J. W., Pompliano, D. L., and Hammond, G. G. (1998) *Chem. Biol. 5*, 185−198.

BI001210R